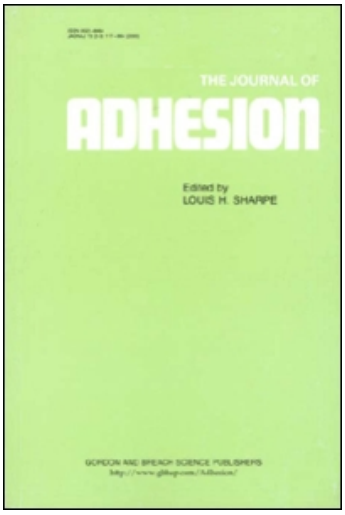


**The Journal of Adhesion**
Publication details, including instructions for authors and subscription information:
http://www.informaworld.com/smpp/title~content=t713453635

# Architecture of the Biomineralized Byssus of the Saddle Oyster (*Anomia* sp.)

Jakob Rostgaard Eltzholtz[a]; Henrik Birkedal[a]
[a] Department of Chemistry and Interdisciplinary Nanoscience Center (iNANO), University of Aarhus, Aarhus C, Denmark

**To cite this Article** Eltzholtz, Jakob Rostgaard and Birkedal, Henrik(2009) 'Architecture of the Biomineralized Byssus of the Saddle Oyster (*Anomia* sp.)', The Journal of Adhesion, 85: 9, 590 — 600
**To link to this Article: DOI:** 10.1080/00218460902996820
**URL:** http://dx.doi.org/10.1080/00218460902996820

*The Journal of Adhesion*, 85:590–600, 2009

ISSN: 0021-8464 print/1545-5823 online
DOI: 10.1080/00218460902996820

Taylor & Francis
Taylor & Francis Group

# Architecture of the Biomineralized Byssus of the Saddle Oyster (*Anomia* sp.)

**Jakob Rostgaard Eltzholtz and Henrik Birkedal**
Department of Chemistry and Interdisciplinary Nanoscience Center (iNANO), University of Aarhus, Aarhus C, Denmark

*Nature displays several solutions to underwater adhesion. In the bivalve mussels, an adhesive attachment organ known as the byssus is often used. In the blue mussel and related species the byssal system consists of a series of byssus threads that are organic in nature. In contrast hereto, the jingle shell,* Anomia *sp., has a single large mineralized byssus that extends through the bottom shell. Here we investigate the architecture and composition of the* Anomia simplex *byssus using scanning electron microscopy and energy dispersive X-ray spectroscopy. We show that the byssus is organized into a hierarchical assembly of crystals and organic matrix. There is a distinct magnesium distribution that is likely to reflect a combination of polymorph and chemical composition control. Sulfur is found to be distributed in distinct zones and sulfur-containing organic matrix provides interconnections between soft tissue and the mineralized byssus. Powder X-ray diffraction shows that calcite and aragonite are present in roughly equal ratios: 55.5(5) wt% aragonite by Rietveld refinement.*



**Keywords:** *Anomia*; Biological adhesion; Byssus; Calcium carbonate; Electron microscopy; Structure

Received 5 January 2009; in final form 31 March 2009.

This paper is dedicated to Prof. J. Herbert Waite. We thank him for his continuous inspiration.

One of a Collection of papers honoring J. Herbert Waite, the recipient in February 2009 of *The Adhesion Society Award for Excellence in Adhesion Science, Sponsored by 3M*.

Address correspondence to Henrik Birkedal, Department of Chemistry and Interdisciplinary Nanoscience Center, University of Aarhus, 140 Langelandsgade, DK-8000 Aarhus C, Denmark. E-mail: hbirkedal@chem.au.dk

## 1. INTRODUCTION

Underwater adhesion is no mean feat but it has been masterfully accomplished by a series of marine organisms. Several bivalves adhere to their preferred substrates through a byssus system. Prime amongst these byssally attached organisms are the mytiloids such as the common blue mussel, *Mytilus edulis*. They are attached through a bunch of threads, the study of which has been pioneered by Waite [1–5]. In the mytiloids, the byssi are organic in nature and the Waite group has unraveled many of the proteins involved in their construction and in the actual adhesion [1–4,6–13]. The mussels use a system of many (several tens of) byssus threads to ensure that there is sufficient resistance to crashing waves in the intertidal zone they inhabit. The adhesion involves proteins rich in the amino acid DOPA (3,5-dihydroxyphenylalanine) [1,3,4,10,12,13]. In contrast to the mussels, the bivalves Anomiidae have but a single byssus thread, which intriguingly is mineralized (with the exception of *Enigmonia*) [14]. The jingle shell, *Anomia* sp., is the only member of the Anomiidae whose byssus has been studied in any detail [15–17]. It is highly mineralized (>90% [16]) by calcium carbonate and both of the $CaCO_3$ polymorphs aragonite and calcite are present [15–17] although their distribution still has not been investigated. The animal attaches to small stones or shells from other mollusks and lies on the side so that the right shell is turned towards the substrate while the left shell is presented to the environment. The calcified byssus is attached to the left valve by retractor muscles [14,17]. In the present paper we investigate the architecture of the byssus of *Anomia simplex* by scanning electron microscopy (SEM) and the chemical composition by energy dispersive X-ray spectroscopy (EDX) and find that there are distinct, detailed design features leading to a complex hierarchical architecture. Powder X-ray diffraction (XRD) is used to show that aragonite and calcite are present in roughly equal quantities and that there are several distinct calcite phases present, presumably due to differences in Mg content.



## 2. EXPERIMENTAL

*Anomia* specimens were obtained from the Department of Marine Resources of the Marine Biological Laboratory, Woods Hole, MA, USA. The specimens were either located on shells or on pebbles.

Byssi were extracted from thawed animals and dehydrated in a graded series of water/ethanol from 70 to 100% dry ethanol (ethanol from Kemetyl A/S, Køge, Denmark). For cross-sectional fracture imaging, byssi were fractured by placing a scalpel in the desired orientation

and tapping it gently with a hammer. In most cases this resulted in essentially pure fractures with only a very small amount of cut surface. The cut surface was visibly flattened by the action of the blade as compared with the fracture surface. Only features originating from the fracture surfaces are reported. They were either imaged in low vacuum, high vacuum with low energy (3–5 keV) electrons, or gold coated and then imaged in high vacuum. All measurements on these samples were performed on a FEI novaSEM 600 field emission SEM (FEI, Eindhoven, The Netherlands). For energy dispersive X-ray analysis (EDX) investigations and back scatter electron imaging (BSE), samples were embedded in Epofix® (Struers A/S, Ballerup, Denmark) and the desired section exposed by polishing with progressively finer SiC paper followed by a final polishing with diamond paste down to a particle size of 0.25 μm. BSE and EDX investigations were conducted on a CamScan MaXim 2040 EnVac SEM (CamScan, Waterbeach, Cambridgeshire, UK).

X-ray powder diffraction data were collected on a single powdered byssus on a Bruker D8 advance powder diffractometer (Bruker AXS GmbH, Karlsruhe, Germany) with Cu$K_{\alpha 1}$ radiation ($\lambda = 1.54056$ Å) in the $2\theta$-range 15–90° in 0.02° steps. Data collected on four different byssi yielded qualitatively similar results. The data were modeled by Rietveld refinement using GSAS [18] with the EXPGUI interface [19]. A two-phase model consisting of an aragonite and a calcite phase was used.



## 2. RESULTS AND DISCUSSION

The *Anomia* byssus of a specimen originating from a pebble is shown in Fig. 1A together with the pulled off animal. When pulling on live

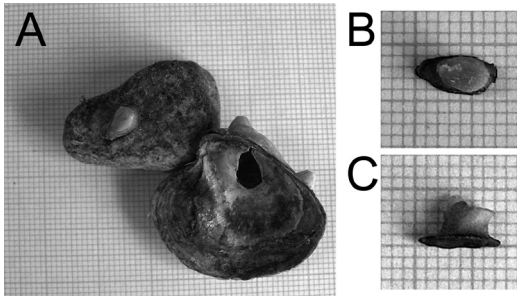


**FIGURE 1** Photograph of (A) an Anomia sp. specimen and (B & C) an extracted byssus from another animal. The specimen was originally attached to a pebble. The specimens were positioned on millimeter paper, each square being 1 × 1 mm. B and C show an isolated byssus from the (B) top and (C) side.

animals perpendicularly to the substrate, failure invariably occurs at the soft tissue/byssus interface and not on the substrate/byssus interface in accordance with previous observations [15]. The byssi proper, which are very light brown in color, are about 2.5 mm tall (Figs. 1B and 1C). They are oval in cross-section (roughly $3 \times 4.5$ mm) while the adhesive footprint, or basal plaque, which is also mineralized but dark brown presumably due to tanning of the organic phase, is larger, roughly $3.5 \times 8$ mm in cross-section (Figs. 1B and 1C). Qualitative observations on the investigated animals show that the actual byssus size scales with the size of the animal as also found by Yamaguchi in his investigations of *A. chinensis* [17].

Figure 2A shows a scanning electron microscopy (SEM) overview image of a byssus seen from the top. The mineralized large basal plaque surrounds the lamellar byssal rod. The folded organic matrix seen on the top is a remnant of the organic matrix extending into the soft tissue of the animal [15,17]. Figure 2B shows an overview of a cross-sectional fracture made in the anterior-ventral direction. The lamellar architecture of the top half of the byssus is clearly displayed. In the bottom third of the byssus, towards the substrate and coinciding in large part with the basal plaque and termed the porous layer by Yamaguchi [17], a different architecture is visible. In this part holes abound. Some of these are also seen from the exterior [15,17] and are involved in interconnection with the surrounding soft tissue [17] while others are not directly in contact with the surroundings. The holes are surrounded by an organic matrix; this holds for both the holes/tubes that are connecting with the outside and the ones restricted to the byssus interior (Figs. 2C–E). Images taken on dorsal-ventral cross-sections show that some, if not all, of the cavities inside the byssus interior are actually also tubes. In some cases, the organic matrix was found to spontaneously come apart revealing that it is laminar and consisting of what appears to be organic sheets (presumably stiff) interconnected by another organic phase seen as stringy filaments in the delaminated organic matrix shown in Figs. 2D and 2E. This design hints at a fracture deflecting purpose of the holes.

The detailed architecture of the byssus was investigated on several byssal cross-sections and fractures. Detailed images of the cross section shown in Fig. 2B are shown in Fig. 3. Figure 3A shows an assembled image from the substrate up to a little more than half of the byssus, height. On the left hand side of the figure, a sketch of the main features is shown. The byssus can be divided into two main zones as a function of distance from the substrate. Close to the substrate the porous layer is found, which in this specimen is on the order of 0.5 mm thick. The thickness of this layer is largest towards the

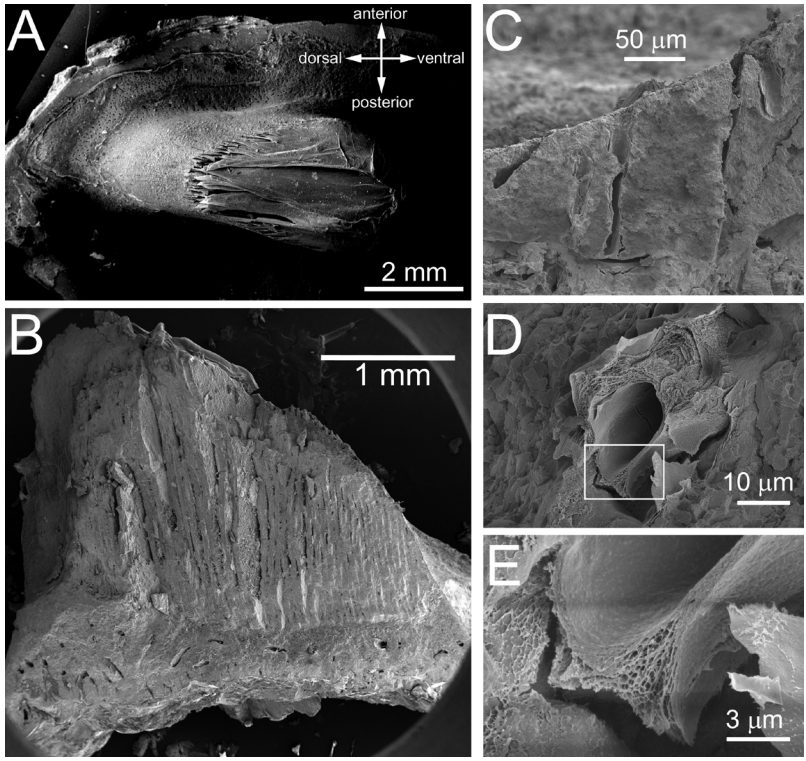


**FIGURE 2** (A) Overview of byssus seen from the top. (B) Fracture surface obtained by fracturing in the anterior-ventral direction. Note the presence of lamellae in the top half of the byssus and the presence of holes in the bottom half. (C) The basal plaque of the byssus is replete with holes that extend towards the substrate and are lined with organic matrix. Image taken from a dorsal-ventral fracture surface; the image shown is from the dorsal end. (D) The organic matrix lining the channels and holes is laminated as shown by this example, where the matrix has delaminated. The image is from the same dorsal-ventral fracture surface used in (C) but from close to the ventral end. (E) Zoom in on (D) in the region marked by the white box in (D).

exterior of the byssus (data not shown, see also [17]). This is then followed by the upper portion of the byssus, which is lamellar in nature. Starting at the substrate interface, we find that the plaque layer consists of deformed spheroidal assemblies of smaller crystals (Figs. 3A and 3E). The size of these assemblies increases when moving up through the byssus (Figs. 3A and 3D). The size of the assemblies ranges from about 5 μm (ranging from 1–2 to 10 μm) towards the substrate to on the order of 35 μm towards the end of the basal plaque

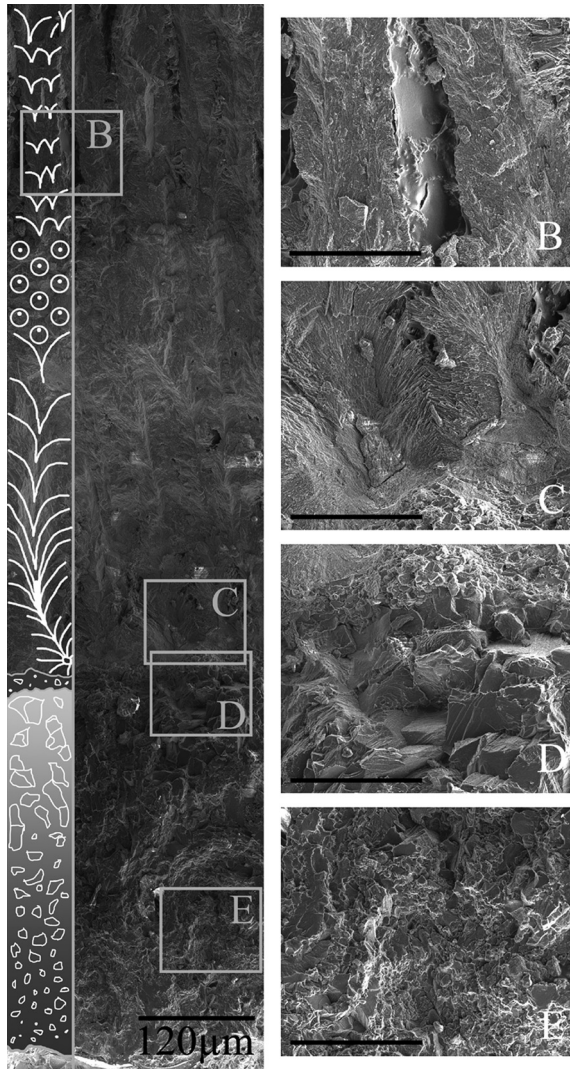


**FIGURE 3** Hierarchical design of the *Anomia* sp. byssus as evidenced by SEM images of a mechanical fracture. (A) Vertical cut through the bottom roughly half of the byssus (composite image). The substrate interface is at the bottom of the image. The primary architectural features have been indicated in the sketch on the left hand side (see text). (B) Zoom in on the upper lamellae in the position indicated by the box labeled B in figure A. (C) Zoom on the lower lamellae/ball region interface. (D) Zoom in on the top part of the ball region. (E) Zoom in on the lower part of the ball region. Images have been digitally regrouped and contrast enhanced. The scale bars in B–E represent 50 μm.

layer. Close to the actual byssus/substrate interface, foreign bodies were sometimes seen such as imprints of diatoms (images not shown). At the border between the porous layer and the lamellar part of the byssus, there is a thin section, roughly 15 μm in width, with smaller assemblies of crystals (Fig. 2C and 2D). Detailed SEM imaging of the spheriodal assemblies show that they are formed of small needle-shaped crystals interconnected by organic matrix (data not shown).

The lamellar part of the byssus can be divided into two subzones separated by an approximately 130-μm transition zone. The bottom one, closest to the basal plaque layer and roughly 250 μm thick, consists of thick lamellae about 50 μm in width. The lamellae contain needle crystal assemblies that splay outwards and upwards from a common axis as shown in Fig. 3C. In between the lamellae, thicker crystals are observed as well as organic matrix. In the ~130 μm transition zone, the orientation of the crystals changes from in plane (Fig. 3A) to point perpendicular to the plane, the "perpendicularity" increasing with distance from the bottom as indicated in the schematic drawing in Fig. 3A by the positions of the dots in the circles, the dot indicating the direction of the vector corresponding to the common crystal orientation. The transition zone then abruptly changes to the upper lamellar zone. Here, the lamellae consist of two rows of splayed out crystals with a thick organic layer in between (Fig. 2B). These organic sheets are dimpled by the presence of crystal protrusions that may play a role in resistance to shear stress. The thicker crystals found between lamellae (Fig. 2A and top right corner of Fig. 2B) are interconnected by organic matrix (data not shown).

We also investigated the chemical composition of the byssi by performing backscattered electron (BSE) imaging and EDX in the SEM. A BSE image of a polished dorsal-ventral cross section is shown in Fig. 4A. The lamellar part of the byssus is replete with mineralized "fingers" that project into the soft tissue as also seen in Fig. 2B. The interfinger space has higher BSE contrast indicating that the interlamellar space has a higher degree of mineralization (Figs. 4A and 4B). This is confirmed by EDX spectroscopy data as shown in Fig. 4B that presents maps of the distribution of Ca, Mg, and S. Calcium is present throughout the byssus, but with slightly larger concentrations between the lamellae. The magnesium distribution is very different. There is essentially no Mg in the top lamellar part of the byssus suggesting that it may be aragonitic, as Mg does not substitute into the aragonite lattice. This result is in accord with staining results of Yamaguchi [17] who found that the lamellae stained with Meigen's solution indicating that they are aragonitic. In the bottom half of the byssus, there is a distinct distribution with the top part just above

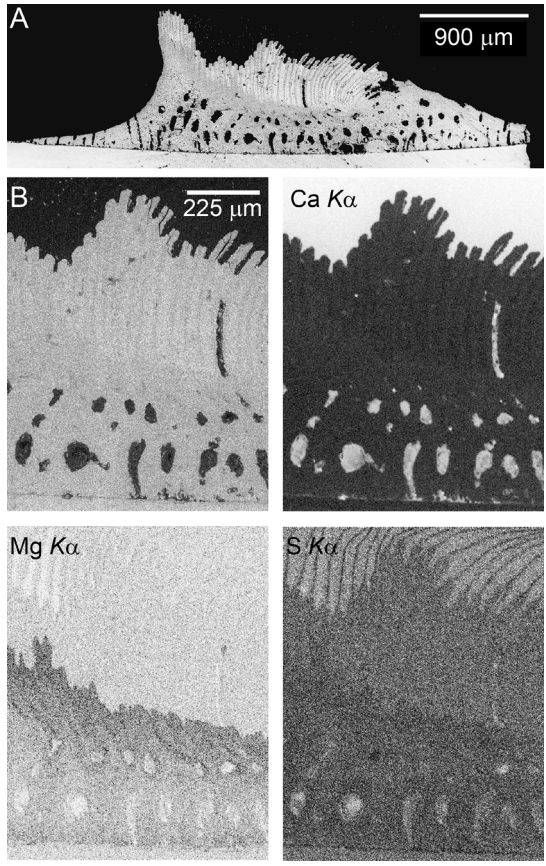


**FIGURE 4** Backscattered electron images and elemental maps of a polished cross section embedded in epoxy. Images and elemental maps recorded with 20 keV electrons. The images have been individually digitally contrast adjusted. For the elemental maps, darker colors signify higher count rate.

the end of the pore layer having a significantly higher Mg content than the pore-containing region. The presence of magnesium in the entirety of the porous zone proves that calcite is present throughout this part of the byssus. The change in the Mg concentration suggests that there may be distinct types of calcite present.

Powder X-ray diffraction data (XRD) from a single byssus are shown in Fig. 5. Both aragonite and calcite are clearly present. A simple two-phase model was fit to the data by Rietveld refinement yielding an aragonite content of 55.5(5) wt%. The calcite peaks display clear shoulders (Fig. 5B). Together with the EDX data discussed above,

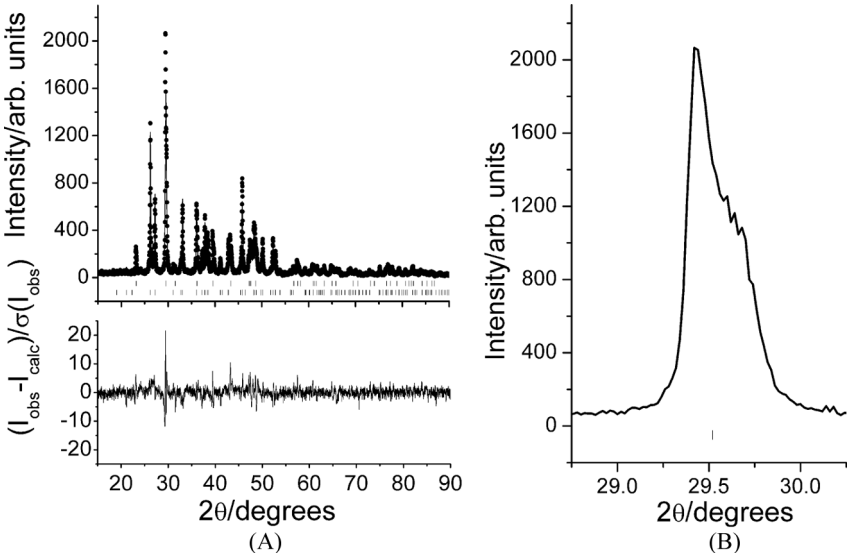


**FIGURE 5** Powder X-ray diffraction analysis of a powdered byssus. (A) Rietveld refinement with a two-phase model containing aragonite and calcite. Top panel: The dots represent the data while the full line is the fit. The calculated positions of the peaks are shown as vertical bars below the data with the top and bottom set representing calcite and aragonite, respectively. Bottom panel: standard uncertainty weighted difference between observed and model intensities in the Rietveld fit; the fit is, in general, good except for the calcite peaks. (B) Plot of the measured calcite (1 0 4) peak; there are very clear shoulders on the high angle side of the main peak reflecting the presence of Mg-rich calcite phases.



these data conclusively establish that there are distinct calcite phases present in the byssus, with a varying Mg content. Full analysis of the XRD data as well as position resolved X-ray diffraction investigations are beyond the scope of the present paper and will be presented in a forthcoming contribution.

The results discussed above show that *Anomia* is not only capable of deciding which calcium carbonate polymorph is formed where and with which shape, but also which substitution chemistry is allowed to take place. This level of control surpasses what is presently feasible in the synthetic systems and shows that we still have much to learn from these "simple" organisms. The sulfur distribution (Fig. 4B), is also interesting. There is clearly an increased S concentration in the byssus compared to the substrate shell (unknown species). The sulfur content is largest in the porous layer and slightly lower in the Mg-rich

region than in the porous part proper. In the lamellar part, projections of sulfur-rich organic matrix is seen (Fig. 4B) to extend from the mineralized fingers into the embedding medium. These projections coincide with the organic sheets seen in Fig. 2A. The organic matrix is, thus, rich in sulfur. This is of interest since it is known that the insoluble fraction of the organic matrix is rich in the sulfur-containing amino acid methionine as well as in sugars [16]. The presence of sugars suggests that sulfur may be present in part as sulfate-substituted polysaccharides known to be involved in biomineralization processes in other organisms [20].

## 4. CONCLUSIONS

The complex microstructure revealed in the present study (Figs. 2–4) brings to light an advanced hierarchical architecture. The presence of holes surrounded by a layered organic matrix in the bottom porous part, which is extended outside the animal, is suggestive of a fracture stopping mechanism. This is further supported by the observation of the lamellar structure of the organic lining surrounding the pores/cavities. The lamellar nature of the top half of the byssus clearly provides a possibility for interconnection with the soft tissue through interweaving. The hard, stiff nature of the highly mineralized byssus makes one ponder how the animal copes with the build up of stress at the soft-tissue/byssus interface where a presumably very stiff, highly mineralized structure meets soft muscular tissue. Waite and coworkers have discussed how gradients are used in biology to reduce this problem with large changes in mechanical properties at interfaces between hard and soft matter [4] and we speculate that the architecture observed in *Anomia* may help alleviate this problem. Whether this holds will be studied by investigations of the mechanical properties of the byssus. Preliminary nanoindentation measurements have revealed that the average indentation hardness and modulus are respectively $\sim$20% higher (hardness) and lower (modulus) than those of single crystal calcite [21].

Comparative studies of the much larger byssus of the related, but evolutionarily more primitive [14], *Pododesmus* species will allow us to determine whether the mesoscopic design principles observed here are present throughout the anomiidae. Such studies are under way.

## ACKNOWLEDGMENTS

Support from the Danish Research Councils through a Steno assistant and a Skou associate professor fellowship to HB is gratefully

acknowledged. We thank Prof. J. Herbert Waite for suggesting undertaking the present study and Dr. James C. Weaver for helpful discussion.

## REFERENCES

[1] Waite, J. H., *Biol. Rev.* **58**, 209–231 (1983).
[2] Waite, J. H., Vaccaro, E., Sun, C., and Lucas, J. M., *Phil. Trans. R. Soc. Lond. B* **357**, 143–153 (2002).
[3] Waite, J. H., *Integr. Comp. Biol.* **42**, 1172–1180 (2002).
[4] Waite, J. H., Lichtenegger, H. C., Stucky, G. D., and Hansma, P., *Biochemistry* **43**, 7653–7662 (2004).
[5] Holten-Andersen, N., Fantner, G. E., Hohlbauch, S., Waite, J. H., and Zok, F. W., *Nature Materials* **6**, 669–672 (2007).
[6] Qin, X.-X., Coyne, K. J., and Waite, J. H., *J. Biol. Chem.* **272**, 32623–32627 (1997).
[7] Qin, X.-X. and Waite, J. H., *Proc. Natl. Acad. Sci. USA* **95**, 10517–10522 (1998).
[8] Waite, J. H., *Comp. Biochem. Physiol. B* **97**, 19–29 (1990).
[9] Hassenkam, T., Gutsmann, T., Hansma, P., Sagert, J., and Waite, J. H., *Biomacromolecules* **5**, 1351–1355 (2004).
[10] Lin, Q., Gourdon, D., Sun, C., Holten-Andersen, N., Anderson, T. H., Waite, J. H., and Israelachvili, J. N., *Proc. Natl. Acad. Sci. USA* **104**, 3782–3786 (2007).
[11] Zhao, H. and Waite, J. H., *Biochemistry* **45**, 14223–14231 (2006).
[12] Zhao, H. and Waite, J. H., *J. Biol. Chem.* **281**, 26150–26158 (2006).
[13] Zhao, H., Robertson, N. B., Jewhurst, S. A., and Waite, J. H., *J. Biol. Chem.* **281**, 11090–11096 (2006).
[14] Yonge, C. M., *Phil. Trans. R. Soc. Lond. B* **276**, 453–523 (1977).
[15] Prezant, R. S., *American Malacological Bulletin* **2**, 41–50 (1984).
[16] Pujol, J. P., Bocquet, J., Tiffon, Y., and Rolland, M., *Calc. Tiss. Res.* **5**, 317–326 (1970).
[17] Yamaguchi, K., *Marine Biology* **132**, 651–661 (1998).
[18] Larson, A. C. and Von Dreele, R. B., General stucture analysis system (GSAS) Report LAUR 86-748 (Los Alamos National Laboratory, Los Alamos, NM, USA, 2000).
[19] Toby, B. H., *J. Appl. Cryst.* **34**, 210–213 (2001).
[20] Mann, S., *Biomineralization: Principles and Concepts in Bioinorganic Materials Chemistry* (Oxford University Principles Press, Oxford, 2001).
[21] Eltzholtz, J. R., Krogsgaard, M., and Birkedal, H. in *Structure-Property Relationships in Biomineralized and Biomimetic Composites*, D. Kisailus, L. Estroff, W. Landis, P. Zavattieri, and H. S. Gupta (eds.) *Mater. Res. Soc. Symp. Proc.* **1187**, KK05-09 (2009).